Research Article Vol. 15, No. 12 / 1 Dec 2025 / Optical Materials Express 3172
Optical Materials EXPRESS

Investigating the stable ductile grinding regime for optical processing using a dicing saw

JOEL M. N. KEEN,[†,*] MATTHEW P. D'SOUZA,[†] PAUL C. GOW, GLENN M. CHURCHILL, CORIN B. E. GAWITH, AND JAMES C. GATES

Optoelectronics Research Centre, University of Southampton, SO17 1BJ, UK
[†]The authors contributed equally to this work.
[*]*j.keen@soton.ac.uk*

Abstract: Ductile grinding on a dicing saw is a viable technique for producing optical waveguides and facets in brittle materials, particularly commercially produced lithium niobate waveguides. However, to date, the literature has focused on empirically defined parameters with little investigation of the grinding dynamics. In this study, we first review the formation of lithium niobate waveguides using a dicing saw to determine what parameters the community is employing. We then perform a series of grinding experiments to explore key process parameters, e.g., cut depth and feed rate, in optical quality grinding of lithium niobate. This work is the first large-distance grinding investigation in this important material. Our literature review shows that the optical dicing community normally finds that optical quality is easy to achieve in ductile mode, though the dynamics of this process are not well defined. However, our work shows that processing speed is limited by the blade wear rate prior to a significant roughness increase. We propose a blade wear-rate transition within the ductile regime, which can be approached by cut depth or feed-rate adjustment. Finding the blade wear-rate transition point provides optimal parameters to maximise throughput with minimal blade wear for the highest manufacturing efficiency.

1. Introduction

Dicing of brittle materials in wafer form is an integral part of the global semiconductor industry. The process is versatile and adaptable, using a rotating abrasive blade and high precision motion stages to machine linear trenches into the material. Although the grinding process for brittle materials is well understood by the machining community for the production of industrial ceramics [1], most dicing processes are developed empirically with the help of the supplier. As a result, very little industrial grinding knowledge has been applied to the specialised dicing process used by the photonics community, i.e "optical dicing". This is used to produce optical quality (nanometre roughness, minimal sub-surface damage) surfaces in brittle materials, such as germanium, silicon and lithium niobate [2]. To achieve roughness this low, a ductile machining regime [3,4] is achieved by using suitably adjusted dicing parameters. It is also common for grinding processes to require additional post-processing, such as polishing or thermal finishing. The recent demonstrations of employing dicing saw systems for optical quality features without post-processing is exceptional. This is particularly useful in devices where post processing is not viable due to the waveguide geometry or form loss from polishing end facets [5].

Prior work in the area of optical dicing has relied upon time-consuming experimental derivation of parameters that provide an acceptable surface finish, consistent form and high process throughput. Previous optical dicing has been carried out to support device fabrication, so characterisation has often been qualitative and has not been optimised for quality or throughput due to lack of understanding of the dynamics of the process. In this paper we present a series

#574264 https://doi.org/10.1364/OME.574264
Journal © 2025 Received 13 Aug 2025; revised 17 Oct 2025; accepted 5 Nov 2025; published 14 Nov 2025

Optical Materials EXPRESS

of investigations into the key processing parameters for optical dicing and relating these to qualitative insight from the ultra-precision grinding field. This work focuses on diced trenches in lithium niobate as the test case, as one of the most publicised platforms using this approach, with images of relevant previous work in Fig. 1. We will also provide a review of the machining parameters used in the literature and comment on their commonalities. Although we focus on lithium niobate here, our findings and suggested strategies for optimising dicing processes can be applied to other photonic platforms.

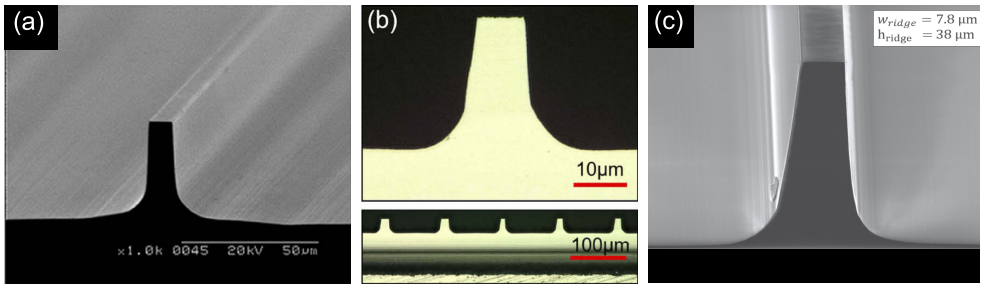

Fig. 1. (a) SEM image of a MgO:PPLN ridge waveguide [6]. (b) Micrograph of a diced facet at 500x and 2000x magnification [7]. (c) SEM image of a diced ridge structure [8]. All reprinted with permission from ©Optica Publishing Group

While there are difficulties associated with processing lithium niobate in a standard cleanroom using techniques such as plasma and chemical etching, very high quality results can be obtained by direct bonding and dry etching as shown by Umeki [9] and Kou [10]. However, for processing bulk lithium niobate and small batch processing without expensive cleanroom equipment, semiconductor dicing saws have been used to form ridge waveguides with great success. This process was pioneered by Kawaguchi [11] and Mizuuchi [12] in the early 2000's, before being expanded on by Kurimura [13], Tadenaga [14] and Suizu [15] a few years later. Carpenter's work [16] optimised the process, which was subsequently commercialised after publication. The success of this process has led to multiple research groups employing an identical approach.

Most published optical dicing work in lithium niobate has been undertaken with a 0.1 - 0.2 mm/s feed-rate and depth of cut of 20-60 µm, see Table 1. These starting parameters are often the lowest available feed-rate and depth-of-cut on the employed dicing machine. Diamond grit size and blade width are not always defined, the most common parameters being # 5000-6000 grit size (equivalent to 1-3 µm) and 0.05 - 0.2 mm blade width. These four parameters are the key controls for achieving optical dicing conditions. This reported range generally seems to obtain low chipping and surface roughness, although these parameters are not always explicitly quantified or stated in the literature. Early publications rarely give any details on the machining process or equipment used.

Blade condition is a key factor for obtaining high-quality surfaces, although it is not often considered in past work due to the challenge of quantifying the blade's condition. Images from published work can, however, provide an indication of blade profile and condition. Waveguides are typically diced with either rounded or squared profile blades. The profile is defined initially by dressing and subsequently through the actual machining process. The blade profile has significant implications for cut quality and the resulting waveguide width. Using rounded blades may be advantageous due to the more gradual cut profile, but the rounding coupled with depth variation from wafer flatness error causes consequent waveguide width errors, critically affecting optical performance. In [20], modelling predicted that waveguide width variation greater than 150 nm halved SHG conversion efficiency, assuming linear variation.

Optical Materials EXPRESS

Table 1. Reviewed publications of lithium niobate optical dicing

Reference #	Width (μm)	Bond	Grit	Machine	Spindle kRPM	Feed (mm/s)	Depth (μm)
[14]							25
[15]	50			DAC-2SP/86			20, 40, 60, 100
[17]	200			DAD321	10	0.2	20, 35, 526
[6]							30
[16]		Resin	#6000	DAD3430	20	0.1	60
		Nickel	#5000				
[7]	100	Resin	#6000	DAD322	20	0.1	25
[18]				DAD3350	10	0.2	
[19]	50, 200			DAD3350	10	0.2	100
[8]	200	Resin	#6000	DAD3430	40	0.05	38

We seek to explore the effect of blade shape and depth on the key parameters for diced trenches in lithium niobate, namely roughness, form and uniformity. Introducing more variables would increase the complexity of the study; other blade parameters, such as blade exposure, preparation and composition, could be studied in future. Machine stability and dynamics are assumed to be fixed for all of these tests; tooling and samples are assumed to be uniform and consistent.

2. Background theory

It is well understood from the machining community that for each individual abrasive cutting grain, the maximum cut depth must be less than the critical cutting depth [4] to achieve ductile mode machining in a brittle material. This critical grain cutting depth is defined by the workpiece material's mechanical properties. Ductile mode machining uses a non-crack propagating cutting motion and reduces roughness and sub-surface damage significantly in brittle materials. Brittle mode machining removes material by fracture rather than smooth cutting. The maximum cutting depth for each grain h_{cu-max} is shown in Eq. (1), which is adapted from Malkin [21] for a dicing saw geometry, shown in Fig. 2. Figure 3 further illustrates the parameters of this system.

$$h_{cu-max} \propto A\sqrt{\frac{v_w}{v_c}}\sqrt{\frac{a_e}{d_{eq}}} \tag{1}$$

Where A is a factor relating to blade grit density and resulting chip geometry, v_w is the workpiece surface speed and v_c is the tool surface speed. d_{eq} is the tool diameter and a_e is the depth of cut, see Figs. 2 and 3. When the depth of cut is too deep or the feed-rate too great, the maximum grain cutting depth exceeds the material critical cutting depth resulting in brittle mode material removal.

Bifano [4] and later Huang [22] both propose formulae for calculating the critical chip thickness in ductile grinding processes from mechanical properties. Our preliminary exploration into the material properties of lithium niobate suggests that a physical scratch test would be preferable to show the ductile to brittle transition under controlled conditions. An ultra precision diamond turning study indicated a critical chip thickness of 23 nm [23]. An indentation study indicates that it is between 105 and 160 nm [24], though indentation, single scratch, diamond turning and grinding experiments should be compared with caution. From our previous results and also the literature (Table 1), it seems that it is not possible to see significant brittle mode effects when dicing with small depths of cut and fine grit blades in lithium niobate. It is much easier to show brittle mode in harder multi-layer photonic platforms such as silicon nitride [5]. We do, however,

Optical Materials EXPRESS

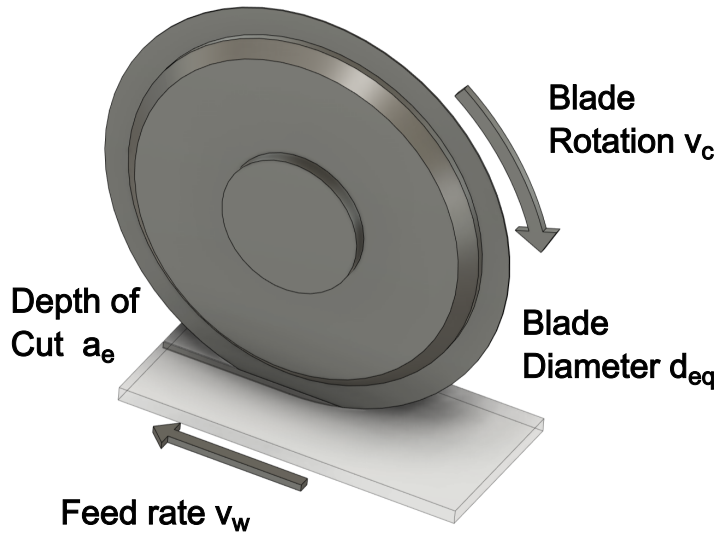

Fig. 2. Schematic of dicing process kinematics and parameters from Eq. (1)

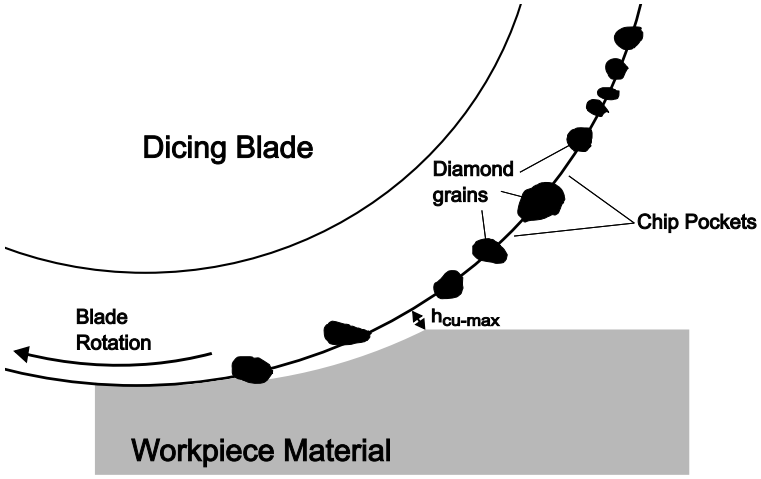

Fig. 3. Diagram of a dicing based diamond grinding process showing multiple grains and chip pockets with the maximum cutting depth for individual grains (h_{cu-max})

see a blade wear-rate transition where the blade starts shedding resin bond and diamond particles, while continuing to cut in ductile mode.

We apply this qualitative insight to our optical grinding to propose two tests for optimising a ductile grinding regime in brittle optical materials towards high throughput and low blade wear. For an otherwise constant parameter set, we propose the blade will wear rapidly in high wear mode until it reaches the cut depth equivalent to the blade wear-rate transition and then continue with minimal blade wear after that point. We further relate blade wear at a constant depth of cut to changes in feed-rate, and predict a similarly significant increase in blade wear at the blade condition transition. These tests could be applied to other brittle photonic materials and ductile grinding processes.

Optical Materials EXPRESS

3. Methodology

Our study includes fabrication of optical grade trenches in z-cut lithium niobate under various conditions to observe the material removal dynamics aiming to provide a general understanding of process dynamics within the ductile regime. From significant previous experience in dicing lithium niobate [2,16,25], we were able to produce an informed parameter range for our investigation, entirely in ductile mode. We had already established sensible stable conditions for productive waveguide machining; however we wished to investigate further to see if potential optimisations were available from varying cut parameters.

We diced many linear metres of trenches with different feed-rates, depths of cut, and blade profiles for subsequent characterisation. Our first investigation tried to relate initial depths of cut and blade shape with resulting cut quality. The spindle speed was 20 krpm with a constant 2 mm/s feed-rate, starting 50 and 100 µm cut depth each with a round and square dressed blade. Subsequently, using knowledge gained from the first investigation, we examined the relationship between feed rate and blade wear. The spindle speed of 20 krpm was retained while the starting cut depth was 40 µm using a square dressed blade only. Across both investigations, the starting depths were chosen to balance the respective requirements of shallow waveguide and deeper facet geometry.

The samples were ground on a DAD3430 (Disco Corporation, JP) dicing saw using a 100 µm wide resin bond blade, with nominal # 6000 (1-2 µm) grit size and 25% diamond concentration. To obtain a square blade profile, we used a hard dressing board (PB08-F30) with a dressing depth of approximately 250 µm, deeper than all previous cuts, to flatten the profile without any sidewall wear. Working empirically, the soft bonded blade required two dressing passes to achieve the desired form. To obtain a round blade, a softer dressing board (PB08-F50) was used. Five passes at 50 µm depth were sufficient to round over the blade profile. Figure 4 shows a sample end facet of square and rounded machined trenches. The cut depth, width, form profile and sidewall roughness were characterised sequentially by Coherence Scanning Interferometry (CSI) on a ZeScope Optical Profiler (Zygo Corp, US).

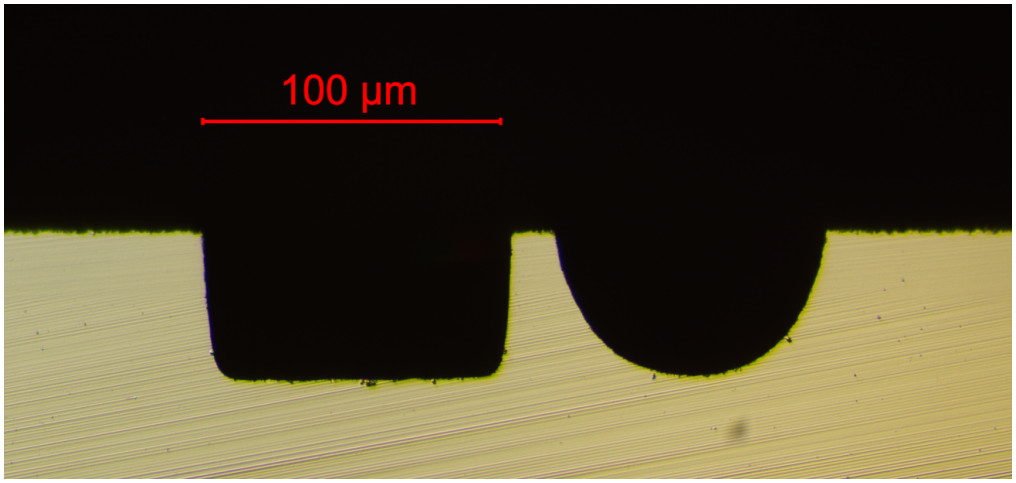

Fig. 4. End-on microscope images of a square (left) and round (right) machined trenches at a programmed 50 µm depth

Figure S1, in the Supplement 1, shows our experimental workflow. Firstly, to normalise cutting conditions, 25 mm by 50 mm rectangular sections were diced out from the wafer to ensure consistency throughout the investigation (S1.1). Using a rectangular sample reduces the likelihood of blade deflection from the curved edge of a full wafer. Secondly, multiple trenches

Optical Materials EXPRESS

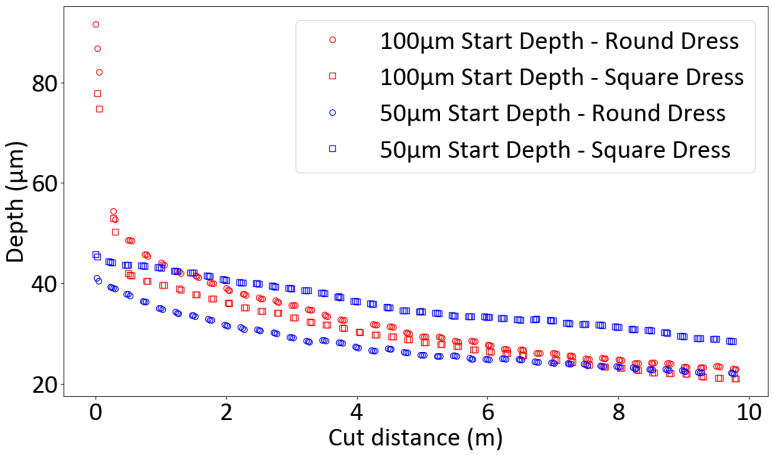

Fig. 5. Trench depth variation against cut distance with constant feed-rate and spindle speed (2 mm/s and 20 krpm)

with a total cut length of 10 m were ground into the standard samples (S1.2). A safe area was left for handling the sample.

Thirdly, a simple top down CSI scan (S1.3) obtained depth and width data. A Python script was used to manually three-point level then automatically datum from the wafer surface. The script performed comparative selections to find the edge. The points were averaged across the trench length, returning the width of the trench. The deepest point for each trench section was also averaged to show depth of cut relative to the datum plane. Fourthly, the samples were then sectioned by cutting a 2 mm wide strip from both entry and exit of each sample (S1.4). The facet surfaces were scanned with the ZeScope with a very short scan depth of 10 µm (S1.5). Finally, the samples were singulated down the middle of every 10 waveguides (S1.6) with a narrower blade. This enabled analysis of the trench sidewalls with the ZeScope (S1.7) to obtain roughness data.

4. Results and analysis

Figure 5 shows the reduction in measured cut depth over a long period of cutting at constant feed-rate. On the 100 µm deep cut series, the blade wears rapidly for the first 0.5 m of cut distance down to around 50 µm cut depth. After this, blade wear rate decreases slowly and comparably to the 50 µm initial cut depth process. This change in blade wear rate suggests there is a significant change in the stability of the machining process, while remaining fully within the ductile mode. We relate this transition back to the idea of individual grain cutting depths in Section 2, Eq. (1); when the force exerted by the cutting depth for a given diamond grain exceeds the bond strength of the dicing blade material, the blade wears by grain pull-out [26]. Our results show that low blade wear conditions can be achieved by optimisation of cutting parameters. For our specific scenario, including machine, blade, material and cutting conditions, we suggest using a feed-rate up to 2 mm/s for depths up to 40 µm.

The 50 µm start depth rounded and square blades show similar results, although the square blade wears significantly more slowly, implying much better form control. Our end facet inspection revealed that the rounded blade with 100 µm start depth wore into a square form within the first few cuts, which explains why there is little difference in results between the round and square dressed blades with a 100 µm starting depth.

The nominal blade width from the manufacturer is 100 µm. The physical width of the blade as measured by a handheld micrometer is 99.7 ±1.5 µm. The trench width variation from the mean

Optical Materials EXPRESS

of each parameter set is shown in Fig. 6, while the raw width data is plotted in Figure S2. In Fig. 6, the anomalous spike in the 50 µm start depth square dress series is the result of a damaged sample area.

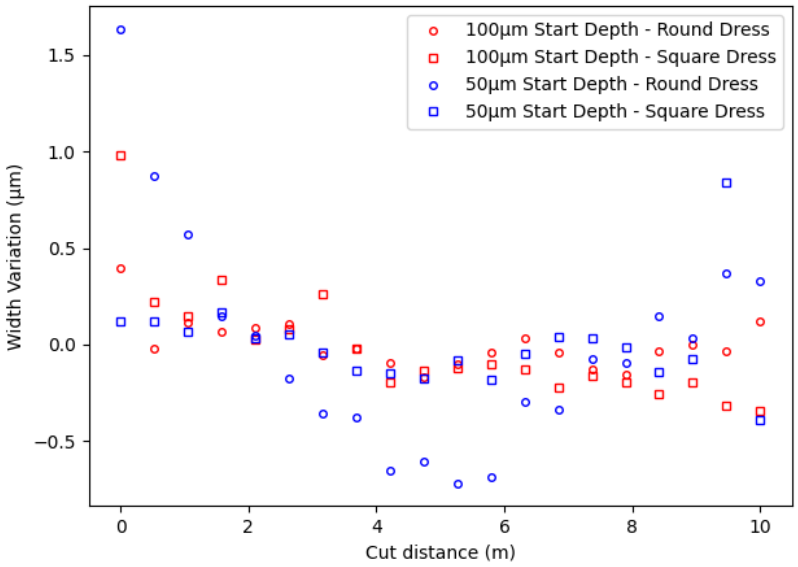

Fig. 6. Trench width variation (normalised to the mean width) against cut distance with constant feed-rate and spindle speed (2 mm/s and 20 krpm)

The trench widths of both square blade processes are similar at around 103 µm. When the profile of rounded blades are used at a depth less than the tip radius, there is a corresponding reduction in cut width. When starting with a 50 µm cut depth and a round dressed blade, the width of cut reduces to around 80 µm, whereas the 100 µm rounded cut depth is only slightly reduced to around 98 µm. We attempted to measure the surface roughness of the trench side walls, but due to the curvature of the side wall profile, measuring the areal surface roughness was not possible. Linear roughness was measured instead. Figure S3 shows the inconclusive vertical Rq roughness from the first phase, we suspect surface contamination on the nano-scale to cause the variability.

In the second phase of the investigation, the sample feed-rate was adjusted to investigate changes in blade wear rate, the results are shown in Fig. 7. This figure shows the average of three cut series which provides some confidence in the repeatability of the blade wear transition. We observe stable wear characteristics until around 2-3 mm/s when a sudden increase in wear rate is observed at the wear rate transition. This is a key parameter for effective production of optical devices with dicing equipment.

Figure 8 shows the vertical Rq roughness from the side walls of these cuts, allowing for missing data points where excessive blade wear prevented reliable measurement. Horizontal Rq roughness would be more useful to compare to the performance of a waveguide as the dominant orientation of scatter loss. However, in our case, the vertical roughness is a good indication that all the cuts were made in the ductile grinding regime. The final cut at 8 mm/s has however significantly higher roughness than the initial cuts, as expected.

Optical Materials EXPRESS

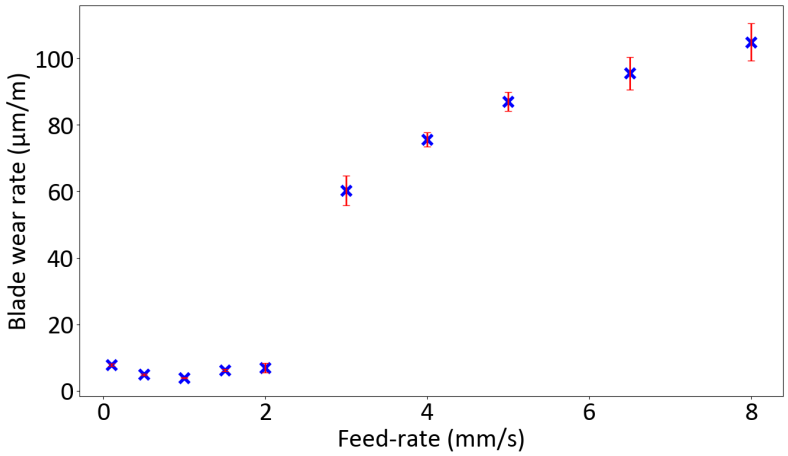

Fig. 7. Blade wear rate variation against feed-rate. The error bars represent the standard deviation of three cut series. Spindle speed 20 krpm, with nominal 40 µm cut depth and square dressed blade.

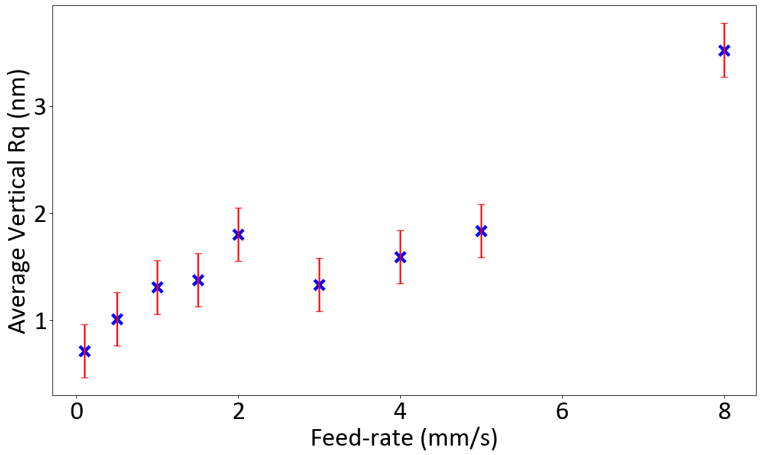

Fig. 8. Side wall roughness variation against feed-rate. The error bars are a fixed value estimating the uncertainty of the measurement system. Spindle speed 20 krpm, with nominal 40 µm cut depth and square dressed blade.

5. Discussion

As expected we were able to observe fully ductile grinding results and a blade wear transition point. Since most brittle material machining processes can only achieve ductile results at the extremity of process capability, not much work has been done on process dynamics within the ductile region. Our results on blade wear show that even when ductile mode is achieved, significant optimisation is required to achieve acceptable results. While the surface roughness we report is suitable for optical applications, the variation between each sidewall and across the feed-rate variation is significant. Our measuring process was operating on the outer limits of its capability in terms of the small sample area and challenging topology.

Chen [27] observes that pockets in between individual abrasive grains on the grinding wheel are important in brittle machining due to the need to remove waste material from the grinding process. We propose that our observed blade wear regime transition is, at least in part, due to

Optical Materials EXPRESS

chip pockets in the dicing blade (see Fig. 3) filling up with removed material, causing the blade to wear. We use a much smaller diamond grain size and which provides very small chip pockets compared to industrial ductile-brittle grinding processes. It is therefore conceivable that the chip pockets in our process would fill up before the ductile-brittle transition, giving a physical explanation for our blade wear transition.

Relating our improved insight into ductile grinding of lithium niobate to the past work reviewed in Table 1, we propose that nearly the entire community is dicing with significantly lower feed rate than the blade wear transition point. All our results were within the ductile cutting mode, from our own surface observations. We propose that all the literature results were also in ductile cutting mode from their published images and also the fact that a brittle cut waveguide would seriously compromise optical function.

We propose future work to investigate the relationship between the blade wear transition and the parameters similar to those in Eq. (1). This would then allow the community to correlate parameters such as feed-rate, maximum cut depth and spindle speed and predict the blade wear transition after initial practical tests.

We also consider that more materials research towards quantifying the critical ductile depth of cut is required, particularly for z-cut lithium niobate. A benchmarked set of scratch tests would improve our understanding of the cutting process after the blade wear transition, while also enabling informed comparisons to be made with other brittle materials.

Individual machine dynamics, such as vibration and motor step resolution, were not investigated in this study and may vary between the various dicing machines in the literature. We expect overall machine stability to be the limiting factor in ductile dicing. The more recent introduction of air bearings for the dicing saw sliding axis as well as the longstanding use of air bearing spindles has coincided with the photonics community adopting dicing saws to produce optical quality waveguides and facets. This also highlights the increasing requirement for a more stable dicing saw with air bearings on all axes, which may improve optical dicing productivity.

6. Conclusion

A dicing saw with low-vibration air bearing spindle running at very high speed ($\geq$ 10 krpm) with a large diameter (50 mm) fine grit ($\geq$ # 5000 or 3 µm) blade and small depth of cut ($\leq$ 50 µm) has been shown to provide consistent ductile machining conditions in lithium niobate. Compared to other machining processes, the comparative ease of achieving ductile conditions even with simple dicing machines is surprising, allowing for optically performant devices to be fabricated with high tolerances relatively simply and easily.

We have investigated optical trench grinding in lithium niobate and presented our findings on the dynamics of the process including blade wear and surface roughness. We show that a simple systematically informed yet rapid set of process tests can be used to optimise existing ductile cutting conditions for generating optical surfaces. This approach can be used to determine stable cutting processes with other dicing parameters and optical materials.

We observed that a square dressed blade in stable wear-rate ductile regime is best for waveguide dimensional consistency when grinding optical surfaces with a dicing saw. This strategy showed that in our specific scenario, including machine, blade, material and cutting conditions, we were able to see low blade wear with a feed-rate up to 2 mm/s for depths up to 40 µm in lithium niobate. This is substantially faster than our previous published work and the wider community, see Table 1.

In future, we intend to investigate the dicing process further in lithium niobate and other brittle optical materials and relate our findings to the grinding equations [4,21]. This work adds to the community's understanding of processes which lead to improvements in the quality and manufacturability of non-linear optical waveguides.

Optical Materials EXPRESS

Funding. Engineering and Physical Sciences Research Council (EP/W024772/1, EP/M013294/1, 2448125, 2928138); Royal Academy of Engineering (RCSRF1718639); Whitworth Society (Senior Award).

Disclosures. The authors declare no conflicts of interest.

Data Availability. All data supporting this study are openly available from the University of Southampton repository at [28].

Supplemental document. See Supplement 1 for supporting content.

References

1. I. D. Marinescu, *Handbook of Advanced Ceramics Machining* (CRC Press, 2006).
2. L. G. Carpenter, C. Holmes, P. A. Cooper, *et al.*, "Precision dicing of optical materials," *Integrated Optics: Devices, Materials, and Technologies XVIII*, vol. 8988 J. E. Broquin and G. N. Conti, eds., International Society for Optics and Photonics (SPIE, 2014), p. 898813.
3. P. A. McKeown, K. Carlisle, P. Shore, *et al.*, "Ultraprecision, high stiffness CNC grinding machines for ductile mode grinding of brittle materials," in *Infrared Technology and Applications*, vol. 1320 (SPIE, 1990), pp. 301–313.
4. T. G. Bifano, T. A. Dow, and R. O. Scattergood, "Ductile-Regime Grinding: A New Technology for Machining Brittle Materials," J. Eng. Ind. **113**(2), 184–189 (1991).
5. P. C. Gow, G. M. Churchill, V. Vitali, *et al.*, "Mechanical dicing of optical quality facets and waveguides in a silicon nitride platform," Electron. Lett. **60**(5), e13138 (2024).
6. J. Sun and C. Xu, "466mW green light generation using annealed proton-exchanged periodically poled MgO:$LiNbO_3$ ridge waveguides," Opt. Lett. **37**(11), 2028–2030 (2012).
7. S. Suntsov, C. E. Rüter, D. Brüske, *et al.*, "Watt-level 775nm SHG with 70% conversion efficiency and 97% pump depletion in annealed/reverse proton exchanged diced PPLN ridge waveguides," Opt. Express **29**(8), 11386–11393 (2021).
8. C. Kießler, M. Kirsch, S. Lengeling, *et al.*, "SPDC single-photon source in Ti-indiffused diced ridge $LiNbO_3$ waveguides," Opt. Continuum **4**(3), 593–606 (2025).
9. T. Umeki, O. Tadanaga, and M. Asobe, "Highly Efficient Wavelength Converter Using Direct-Bonded PPZnLN Ridge Waveguide," IEEE J. Quantum Electron. **46**(8), 1206–1213 (2010).
10. R. Kou, S. Kurimura, K. Kikuchi, *et al.*, "High-gain, wide-dynamic-range parametric interaction in Mg-doped $LiNbO_3$ quasi-phase-matched adhered ridge waveguide," Opt. Express **19**(12), 11867–11872 (2011).
11. T. Kawaguchi, T. Yoshino, J. Kondo, *et al.*, "High-power blue/violet QPM-SHG laser using a new ridge-type waveguide," in *Conference on Lasers and Electro-Optics*, (Optica Publishing Group, 2001), p. CTuI6.
12. K. Mizuuchi, T. Sugita, K. Yamamoto, *et al.*, "Efficient 340-nm light generation by a ridge-type waveguide in a first-order periodically poled MgO:$LiNbO_3$," Opt. Lett. **28**(15), 1344–1346 (2003).
13. S. Kurimura, Y. Kato, M. Maruyama, *et al.*, "Quasi-phase-matched adhered ridge waveguide in LiNbO3," Appl. Phys. Lett. **89**(19), 191123 (2006).
14. O. Tadanaga, T. Yanagawa, Y. Nishida, *et al.*, "Widely tunable 2.3 μm-band difference frequency generation in quasiphase-matched $LiNbO_3$ ridge waveguide using index dispersion control," J. Appl. Phys. **102**(3), 033102 (2007).
15. K. Suizu and K. Kawase, "Monochromatic-Tunable Terahertz-Wave Sources Based on Nonlinear Frequency Conversion Using Lithium Niobate Crystal," IEEE J. Sel. Top. Quantum Electron. **14**(2), 295–306 (2008).
16. L. Carpenter, S. Berry, and C. Gawith, "Ductile dicing of $LiNbO_3$ ridge waveguide facets to achieve 0.29nm surface roughness in single process step," Electron. Lett. **53**(25), 1672–1674 (2017).
17. N. Courjal, B. Guichardaz, G. Ulliac, *et al.*, "High aspect ratio lithium niobate ridge waveguides fabricated by optical grade dicing," J. Phys. D: Appl. Phys. **44**(30), 305101 (2011).
18. M. Mwangi, F. Behague, A. Coste, *et al.*, "In-situ phase control of a low-loss membrane-based lithium-niobate polarisation-state modulator," Opt. Continuum **1**(12), 2513–2520 (2022).
19. R. Zamboni, L. Gauthier-Manuel, A. Zaltron, *et al.*, "Opto-microfluidic coupling between optical waveguides and tilted microchannels in lithium niobate," Opt. Express **31**(17), 28423–28436 (2023).
20. M. Chauvet, F. Henrot, F. Bassignot, *et al.*, "High efficiency frequency doubling in fully diced $LiNbO_3$ ridge waveguides on silicon," J. Opt. **18**(8), 085503 (2016).
21. S. Malkin, *Grinding Technology Theory* (Ellis Horwood Ltd, Publisher, Harlow, England, 1989).
22. H. Huang, B. R. Lawn, R. F. Cook, *et al.*, "Critique of materials-based models of ductile machining in brittle solids," J. Am. Ceram. Soc. **103**(11), 6096–6100 (2020).
23. B. A. Fuchs, C. Syn, and S. P. Velsko, "Diamond turning of lithium niobate for optical applications," Appl. Opt. **31**(27), 5788–5793 (1992).
24. H. Zheng, D. Wen, F. Kong, *et al.*, "Research on critical load of lithium niobate crystal lapping," Processes **10**(5), 912 (2022).
25. L. G. Carpenter, S. A. Berry, A. C. Gray, *et al.*, "CW demonstration of SHG spectral narrowing in a PPLN waveguide generating 2.5 W at 780 nm," Opt. Express **28**(15), 21382–21390 (2020).
26. B. Azarhoushang, I. D. Marinescu, W. B. Rowe, *et al.*, *Tribology and Fundamentals of Abrasive Machining Processes* (William Andrew, 2021).
27. S.-T. Chen and S.-J. Lin, "Development of an extremely thin grinding-tool for grinding microgrooves in optical glass," J. Mater. Process. Technol. **211**(10), 1581–1589 (2011).

Optical Materials EXPRESS

28. J. N. M. Keen, M. P. D'Souza, P. C. Gow, *et al.*, "Investigating the stable ductile grinding regime for optical processing using a dicing saw: data," University of Southampton, 2025, https://doi.org/10.5258/SOTON/D3614